Application of the chiral forces to elctroweak processes

Vitalii Urbanevych

Ph.D. thesis written under the supervision of dr. hab Roman Skibiński
at the Jagiellonian University, Faculty of Physics, Astronomy
and Applied Computer Science, Kraków,
Sunday 3rd October, 2021

CONTENTS

CHAPTER 1

PLAN

- Why we study few nucleon systems
  - Strong interactions (2N and 3N force investigation; QCD, relativistic effects)
  - Electro-magnetic processes (electrons-, photons-induced reactions) (Arenhovel did ...)
  - Weak interactions (neutrons)
- Nuclear forces used in the thesis
  - AV18
  - Chiral (scs, sms; difference between chiral models; regularization problem)
- Currents used in the thesis (regularization of currents to be done)
- Formalism & numerical methods
  - Lippman-Schwinger eq
  - Schrodinger eq for deuteron; wave functions (sms) for deuteron - figures, binding energy
  - Three body: Fadeev eq. for bound (He3, H3) and scattering states
  - Siegert theorem ?
  - Partial wave decomposition, states ($pq\alpha$), Jakobi momenta; operators in PW decomp. (current); Mathematica for PW
  - Theoretical uncertainties: truncation error, cut-off dependency, chiral order dependency
- Results (**find everything what I have calculated: all processes and energies**)
  - H2 photodisintegration
  - He3 and H3 photodisintegration
  - Pion capture

- Summary
- References

Why we study few nucleon systems

The study of light nuclei for the decades has been serving as an easiest way to study NN systems and forces inside the atom. And convenient way to proceed may be an interaction of atom with other particles: elastic or inelastic scattering. It is possible to construct such an experiments and check if theory works. People take into account that interactions may be caused by different forces and therefore should be described in different ways. It can be either strong, weak or electromagnetic interaction. It depends on the type of particle being scattered and the target which reaction it is.

In order to proper describe the nuclear reactions many factors should be taken into account. First of all, different nuclear forces may act on the participants.

The strong nuclear force appear inside the nuclei and among others bound neutrons and protons together. The description of strong interactions is extremely difficult as it deals not only with nucleon, but with their constituents: quarks and gluons. Quantum Chromodynamics(QCD) is a modern theory describing strong interactions, but it has also its limitations at the moment as it is not reliable at low energies ($Q^2 \lesssim 1GeV^2$). So other approaches are coming into the scene such as chiral effective theory, lattice calculation and others [1].

Electromagnetic force appears between charged particles like protons and electrons. Also, the force is transferred between charged particles with a photon, so in photon- and electron- scatterings on the nuclei an electromagnetic force is playing an important role. Arenhovel [2] studied electromagnetic process - Deuteron photodisintegration, applying different approaches and comparing the results with experimental data.

The weak force...

...

Starting the study of 3- (and more) nucleon systems it was found that 2N force is not enough to describe the system and 3N force was introduced. The first applications of such a force showed that it brings sufficient contribution and cannot be ignored [3]. Whereas the first applications included only early "realistic" potential, the latter investigations only proved this statements [4, 5]. It was also used to construct four-nucleon (4N) bound state [6].

...

Nuclear forces used in the thesis

In order to construct a potential people often use phenomenological or semi-phenomenological approaches. It allows to combine theoretical knowledge about processes and experimental data.

One of such potentials, which was used in current thesis is Argonne V18 (AV18) [7] In order to construct NN force, authors combine analytical electromagnetic and one-pion-exchange parts with phenomenological one, fitting parameters to the Nijmegen partial-wave analysis of pp and np data [8]. Authors showed, that AV18 potential delivers good results in the description of nucleon scattering data as well as deuteron properties.

In the early 1990-ies Weinberg [9, 10] introduced an idea of using a most general Lagrangian satisfying assumed symmetry principles and in particular spontaneously broken

chiral symmetry to describe nuclear interactions at low energies. This idea together with effective field theory (EFT) of Quantum chromodynamics (QCD) led to the development of Chiral effective field theory (χEFT) which nowadays has become one of the most advanced approach to describing nuclear reactions at low energies.

For the EFT it is very important to define a quantity, which powers will determine a perturbation order. In the χEFT there are two natural scales: so-called soft scale - the mass of Pion $Q \sim M_\pi$ and hard scale - $\Lambda_\chi \sim 1\ GeV$ (chiral symmetry breaking scale). The ratio between these two scales $(Q/\Lambda_\chi)^\nu$ is being used as an expansion parameter in χEFT with power ν.

Considering so-called irreducible (the diagrams that cannot be split by cutting nucleon lines), Weinberg [9, 10] came to the identity for the powers of such diagrams [11]:

$$\nu_W = 4 - A - 2C + 2L + \sum_i \Delta_i, \tag{1.1}$$

where

$$\Delta_i \equiv d_i + \frac{n_i}{2} - 2 \tag{1.2}$$

In 1.1, C is a number of pieces which are connected, L - the number of loops in the graph. In 1.2, n_i is a number of nucleon field operators, d_i - the number of insertions (or derivatives) of M_π.

In χEFT the first order is called "leading order" (LO) and it is followed by next-to-leading order (NLO), next-to-next-to-leading order (N2LO) and so on. At the moment, the highest order for which there is a derived term in potential is N4LO. Also some contributions from N5LO are included in the N4LO+ chiral order.

As pointed above, for many-nucleon systems it is important to include not only nucleon-nucleon interaction to the potential, but also a 3- and many- nucleon contributions. In the χEFT 3N force contributes starting from N2LO and 4N force is presented starting from N3LO, so there is a systematic way to include all the forces from simplest diagrams at LO and gradually adding more and more terms. It is also beneficial in the way that one can obtain results using chiral potential at different orders and track which one gives larger or smaller contribution (changes in the final results).

The χEFT may be applied both in coordinate and momentum spaces. Nevertheless in both cases it requires regularization which is cutting low coordinate values in order to avoid infinities (or high momentum values - in momentum space). The value at which the cut is applied (cut-off value) is not fixed and usually calculations are being performed for different cut-off values. The comparison of such results may reveal stronger or weaker dependance and in perfect case one will come up with such a potential, were the cut will not affect results much.

The potential may be transformed from coordinate to momentum space (or vice versa), but it is important at which frame the regularization was performed and what was a regularization function. That's why there are different versions of chiral potential. One is semi-local coordinate space regularized potential (SCS) [12] and another one is similar, but with regularization applied in momentum space (SMS potential) [13].

Currents

CHAPTER 2

FORMALISM & NUMERICAL METHODS

In order to calculate any observable for the Deuteron photodisintegration, one has to find a nuclear matrix elements:

$$N^{\mu} = \langle \Psi_f \vec{P}_f \mid \frac{1}{e} J^{\mu}(0) \mid \Psi_i \vec{P}_i \rangle = \langle p'(l's')j'm'_j t'm'_t \vec{P}_f \mid J^{\mu} \mid \phi_d m_d \vec{P}_i \rangle, \tag{2.1}$$

where J^{μ} is a four-vector current operator which acts between initial and final two-nucleon states.

2.1 Deuteron bound state

Let's find a deuteron bound state wave function ϕ_d. The time-independent Schrodinger equation for two particles in such case will be:

$$(H_0 + V) \mid \psi_{12} \rangle = E_d \mid \psi_{12} \rangle \tag{2.2}$$

H_0 is a kinetic energy of the nucleons and V is a potential. The kinetic energy H_0 can be represented in terms of relative and total momenta of the particles:

$$H_0 = \frac{\vec{p}_1^{\,2}}{2m_1} + \frac{\vec{p}_2^{\,2}}{2m_2} = \frac{\vec{p}^{\,2}}{2\mu} + \frac{\vec{\mathcal{P}}^2}{2M}, \tag{2.3}$$

where relative and total momenta are defined as follows:

$$\vec{p} = \frac{(m_1\vec{p}_1 - m_2\vec{p}_2)}{m_1 + m_2} \tag{2.4}$$

$$\vec{\mathcal{P}} = \vec{p}_1 + \vec{p}_2 \tag{2.5}$$

and $M = m_1 + m_2$ is a total mass, $\mu = \frac{m_1 m_2}{M}$ is a relative mass of two nucleons.

We are working in the momentum space, so acting by the momentum operator on the Eq.(2.2) one can obtain two separated equations:

$$\frac{\vec{p}^2}{2\mu}\langle\vec{p}\mid\Psi_{int}\rangle+\int d\vec{p}'\langle\vec{p}\mid V\mid\vec{p}'\rangle\langle\vec{p}'\mid\Psi_{int}\rangle=(E_d-E_{c.m.})\langle\vec{p}\mid\Psi_{int}\rangle \tag{2.6}$$

$$\frac{\vec{\mathcal{P}}^2}{2M}\langle\mathcal{P}\mid\Psi_{c.m.}\rangle=E_{c.m.}\langle\mathcal{P}\mid\Psi_{c.m.}\rangle \tag{2.7}$$

Eq.(2.6) is basically a Schrodinger equation for one particle with mass μ and Eq.(2.7) can be regarded as a Schrodinger equation for particle with mass M in a free motion. Assuming that deuteron is at rest ($E_{c.m.}=0$) we can stick to the Eq.(2.6) only. So that:

$$\frac{\vec{p}^2}{2\mu}\langle\vec{p}\mid\Psi_{int}\rangle+\int d\vec{p}'\langle\vec{p}\mid V\mid\vec{p}'\rangle\langle\vec{p}'\mid\Psi_{int}\rangle=E_d\langle\vec{p}\mid\Psi_{int}\rangle \tag{2.8}$$

Next we move to the partial-wave representation of the momentum state in the following form:

$$\mid\vec{p}\rangle=\mid p\alpha\rangle\equiv\mid p(ls)jm_j\rangle\mid tm_t\rangle, \tag{2.9}$$

where we introduce quantum numbers l, s ,j ,t as orbital angular momentum, total spin, total angular momentum and total isospin respectively. m_j and m_t are isospin and spin projections.

Yet one can introduce simpler states than it is in (2.9).

$$\mid p(ls)jm_j\rangle=\sum_{m_l}c(lsj;m_l,m_j-m_l,m_j)\mid plm_l\rangle\mid s\ m_j-m_l\rangle \tag{2.10}$$

Also we can decompose spin and isospin states as follows:

$$\mid sm_s\rangle=\sum_{m_1}c(\frac{1}{2}\frac{1}{2}s;m_1,m_s-m_1,m_s)\mid\frac{1}{2}m_1\rangle\mid\frac{1}{2}m_s-m_1\rangle \tag{2.11}$$

$$\mid tm_t\rangle=\sum_{\nu_1}c(\frac{1}{2}\frac{1}{2}t;\nu_1,m_t-\nu_1,m_t)\mid\frac{1}{2}\nu_1\rangle\mid\frac{1}{2}m_t-\nu_1\rangle \tag{2.12}$$

In Eqs.(2.10) -(2.12), $c(...)$ are Clebsh-Gordon coefficients. Nucleons are spin $\frac{1}{2}$ particles, and also we treat proton and neutron as the same particle in different isospin states, so that isospin is $\nu_1=\frac{1}{2}$ for proton and $\nu_1=-\frac{1}{2}$ for neutron.

The states $\mid plm_l\rangle$ from Eq.(2.10) are orthogonal, so that

$$\langle p'l'm_l'\mid plm_l\rangle=\frac{\delta(p-p')}{p^2}\delta_{ll'}\delta_{m_lm_l'} \tag{2.13}$$

and also satisfy the completeness relation:

$$\sum_{l=0}^{\infty}\sum_{m_l=-l}^{l}\int dpp^2\mid plm_l\rangle\langle plm_l\mid=\mathbb{1} \tag{2.14}$$

These states also fulfill a relation

$$\langle\vec{p}'\mid plm_l\rangle=\frac{\delta(|\vec{p}'|-p)}{p^2}Y_{lm_l}(\hat{p}'), \tag{2.15}$$

where $Y_{lm_l}(\hat{p}')$ is a spherical harmonic and 'hat' means a unit vector.

If we exchange nucleons 1 and 2 there should be a sign change and this requirement can in mathematical form can be expressed as:

$$(-1)^{l+s+t} = -1 \tag{2.16}$$

Taking into account Eq.(2.16), one can find only one possible case for the deuteron bound state: 2 coupled channels for l=0,2; s=1; j=1and $t = m_t = 0$. These 2 channels are usually denoted as ${}^3S_1$ and ${}^3D_1$ and corresponding wave functions are $\phi_0(p)$ and $\phi_2(p)$.

So with a new basis Eq.(2.8) takes a form:

$$\frac{\vec{p}^2}{2\mu}\phi_l(p) + \sum_{l'=0,2}\int dp' p'^2 \langle p l m_l \mid V \mid p' l' m_l' \rangle \phi_{l'}(p) = E_d \phi_l(p), \tag{2.17}$$

for $l = 0, 2$. Assuming that one has a matrix elements for the potential $\langle p l m_l \mid V \mid p' l' m_l' \rangle$, there is still one complication in the Eq.(2.17) - integration. In order to get rid of the integral I use a Gaussian quadrature method of numerical integration [14]. It allows to replace an integral by the weighted sum: $\int_a^b f(x)dx = \sum_{i=1}^n \omega_i f(x_i)$ In current work I used 72 points in the interval from 0 to $50fm$. Using this method, Eq.(2.8) becomes

$$\frac{\vec{p}^2}{2\mu}\phi_l(p) + \sum_{l'=0,2}\sum_{j=0}^{N} \omega_j p_j'^2 \langle p_j l m_l \mid V \mid p_j' l' m_l' \rangle \phi_{l'}(p) = E_d \phi_l(p), \tag{2.18}$$

It is possible to solve this equation as an eigenvalue problem $M\Psi = E_n\Psi$ and find simultaneously wave function values and binding energy E_n.

2.2 2N scattering state

2.2.1 The Lippman-Schwinger equation

Let us start from the time-independent formulation of the scattering process. In such a case Hamiltonian will be:

$$H = H_0 + V, \tag{2.19}$$

where H_0 is a kinetic energy operator $H_0 = \frac{\vec{p}^2}{2m}$. For a free particle motion, V will be absent and we will denote an energy eigenstate as $\mid \vec{p} \rangle$ - a free particle state. In the case of the scattering process, the eigenstate will differ from $\mid \phi \rangle$, but in case of elastic scattering (which we re interested in) the energy eigenvalue E should be the same.

So below I write a system of Schrodinger equations for such scattering process:

$$\begin{cases} H_0 \mid \vec{p} \rangle & = E \mid \vec{p} \rangle \\ (H_0 + V) \mid \psi \rangle & = E \mid \psi \rangle \end{cases} \tag{2.20}$$

I would like to find such a solution to Eq. (2.20), so that $\mid \psi \rangle \rightarrow \mid \vec{p} \rangle$ with $V \rightarrow 0$ and both $\mid \psi \rangle$ and $\mid \vec{p} \rangle$ have the same energy eigenvalues E. As we have scattering process, the energy spectra for both operators H_0 and$H_0 + V$ are continuous.

From Eq. (2.20) follows that

$$\mid \psi \rangle = \frac{1}{E - H_0} V \mid \psi \rangle + \mid \vec{p} \rangle, \tag{2.21}$$

where $\mid \vec{p}\rangle$ was added artificially in order to satisfy a criterion mentioned above and following the logic from [15]. In addition, it guarantees that application of the operator $(E - H_0)$ to the (2.21) results in the second equation from the system (2.20).

In order to deal with a singular operator $\frac{1}{E-H_0}$ in eq.(2.21), the well-known technique is to make such an operator slightly complex by adding small imaginary number to the denominator so Eq.(2.21) becomes

$$|\psi\rangle = G_0(E \pm i\epsilon)V \mid \psi\rangle + \mid \vec{p}\rangle, \tag{2.22}$$

where G_0 is a free propagator:

$$G_0(z) = \frac{1}{z - H_0} \tag{2.23}$$

Solution with $G_0(E-i\epsilon)$ corresponds to the incoming spherical wave, while $G_0(E-i\epsilon)$ - to the outgoing one. Since we are interested in the scattering process, we will use the $(+)$ sign further.

Eq. (2.22) is known as a Lippman-Schwinger equation (LSE) and using the definition of the transition operator t:

$$t\,|\vec{p}\rangle = V\,|\psi\rangle \tag{2.24}$$

we can rewrite it as

$$|\psi\rangle = (1 + G_0(E + i\epsilon)Vt)\,|\vec{p}\rangle \tag{2.25}$$

With substitution of Eq. (2.22) into Eq. (2.24) we can find an explicit form of the t operator:

$$\begin{aligned} t\,|\vec{p}\rangle &= VG_0(E + i\epsilon)V \mid \psi\rangle + V \mid \vec{p}\rangle = \\ &= VG_0(E + i\epsilon)t\,|\vec{p}\rangle + V \mid \vec{p}\rangle \end{aligned} \tag{2.26}$$

Getting rid of the initial state $|\vec{p}\rangle$ in the Eq. (2.26) we can get a LSE for the transition operator in the iterative form:

$$\begin{aligned} t &= V + VG_0Vt = \\ &= V + VG_0V + VG_0VG_0Vt = ... \end{aligned} \tag{2.27}$$

Using Eq. (2.25) we can write Eq. (2.1) as

$$N^\mu = \langle \phi m_p m_n |\,(1 + G_0(E + i\epsilon)Vt)\frac{1}{e}J^\mu(0) \mid \Psi_i \vec{P}_i\rangle \tag{2.28}$$

2.3 3N scattering state

2.4 Theoretical uncertainties

Truncation error

As it was mention above, each subsequent order of chiral expansion provide us with more and more sophisticated potential. Starling from the leading order (LO) and coming to next N2LO, N3LO and so on we toke into account more Feynmann diagrams and in result potential is able to provide us with more precise predictions for the regarded process and observable. But the chiral expansion (as any expansion) in principle can be continued to the infinity, improving the resulting series. In practice we are limited by some number of terms, but we would like to find out the uncertainty appearing from cutting off remaining part of the expansion. This uncertainty is called a truncation error and there some ways of estimation its value for the potential of each order of chiral expansion having predictions for some limited number of terms [12, 16–18].

Let's regard some observable $X^i(p)$ which is calculated at i-s order of chiral expansion with expansion parameter Q $(i = 0, 2, 3...)$[1]. Here p specifies ????? a momentum scale of the current reaction in the center of mass frame (in the case of deuteron photodisintegration it would be a photon's momentum).

If I define a difference between observable at each subsequent orders as:

$$\Delta X^{(2)} = |X^{(2)} - X^{(0)}|, \Delta X^{(i>2)} = |X^{(i)} - X^{(i-1)}|, \tag{2.29}$$

then chiral expansion for X can be written as:

$$X = X^{(0)} + \Delta X^{(2)} + \Delta X^{(3)} + ... + \Delta X^{(i)} \tag{2.30}$$

The truncation error at order i $\delta X^{(i)}$ is estimated using actual and expected values of the observable at higher orders. In order to do that I use following expressions:

$$\delta X^{(0)} = Q^2 \left|X^{(0)}\right| \tag{2.31}$$

$$\delta X^{(i)} = \max_{2\leq j\leq i} \left(Q^{i+1} \left|X^{(0)}\right|, Q^{i+1-j} \left|\Delta X^{(j)}\right|\right) \tag{2.32}$$

Additionally, following the [17] I use the actual high-order predictions in order to specify uncertainties so that:

$$\delta X^{(i)} \geq \max_{j,k}(|X^{j\geq i} - X^{k\geq i}|) \tag{2.33}$$

and to be conservative I use additional restriction:

$$\delta X^{(i)} \geq Q\delta X^{(i-1)} \tag{2.34}$$

In Fig. 2.1 I present a total cross-section for the deuteron photodisintegration at 3 photon energie values: 30,100 and140 MeV as a dependance on the chiral order. Error bands show truncation errors calculated using described above method. One can see that

[1] We do not have a first order of expansion because this term in chiral expansion is always vanished and NLO corresponds to the quadratic term (number 2)

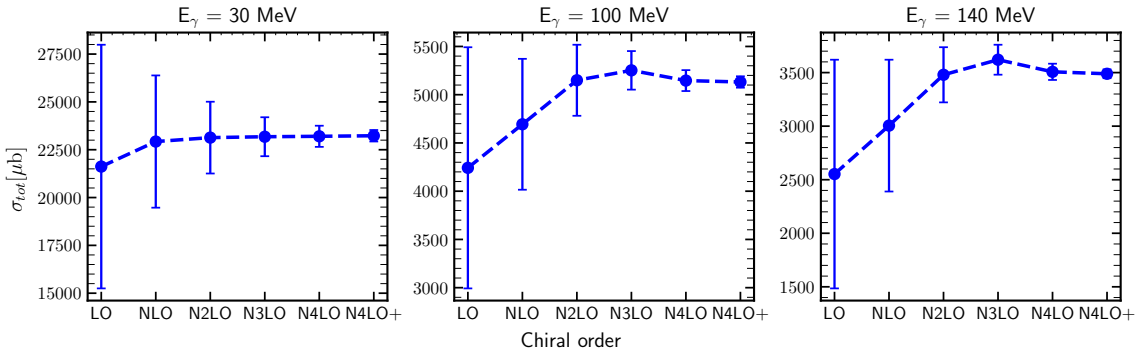

Figure 2.1: Total cross section of the deuteron photonisintegration process as a dependance on the chiral order for three photon energy E_γ values: 30, 100 and 140 MeV. Error bands show an estimated truncation error at each order.

errors are being reduced with each consecutive chiral order: for LO it is the biggest while for N4LO+ it is hardly visible at presented scale.

Cutoff dependency

Another uncertainty comes from the choice of the cutoff parameter's value. According to [13], where the SMS potential was presented, 4 values of the cutoff parameter Λ are recommended: 400, 450, 500 and 550 MeV. Using each of them one obtains different predictions which may differ from actual (experimental) value. Therefore the choice of Λ value may affect a quality of the prediction.

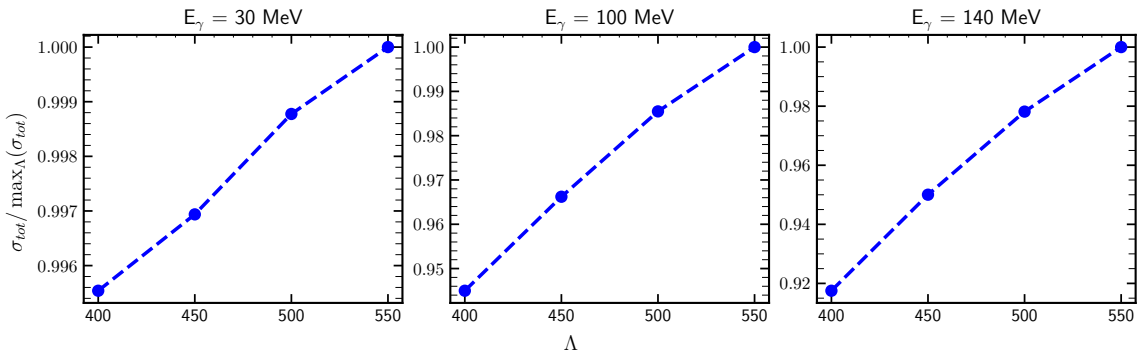

Figure 2.2: Total cross section of the deuteron photonisintegration process as a dependance on the cutoff parameter Λ for three photon energy E_γ values: 30, 100 and 140 MeV.

CHAPTER 3

PION ABSORPTION AT THE LOWEST ATOMIC ORBITAL IN ^{2}H, ^{3}H AND ^{3}HE

CHAPTER 4

RESULTS

4.1 Deuteron photodisintegraion

4.1.1 Cross section

In this section I will show the results of my calculation starting from the deuteron photodisintegration process. One of the most studying observable is obviously cross section. There is a number of papers which present measurement results for both differential and total cross section [19–27] so it is convenient to prepare a theoretical predictions in order to compare it with experimental results.

On the Fig. 4.1 and Fig. 4.2 I present predictions for the total cross section σ_{tot} [μb] which I obtained using the chiral potential at the order N^{4}LO+ and with the cut off parameter $\Lambda = 450$ MeV (my best predictions). Looking at Fig. 4.2, we can see that at low photon energies (below 50 MeV) my predictions which include 2N contributions using Siegert approach, describe experimental results quite well. We can suppose that the difference with experimental data may come from the statistical uncertainty of the data itself, as my predictions are often in between the data from different sources. Moreover even at such low energies the 1N current is clearly not enough to describe this observable as dashed pink line has much lower values and the difference becomes even larger with larger photon's energies.

Having look at the higher energies (above 50 MeV, Fig. 4.1) we can notice that the difference with experimental data is not only quantitative, but also qualitative. There is a peak around 300 MeV in the experimental data from [24] which is not reflected in my predictions. The reason of such discrepancy is most likely coming from the relativistic effects which I do not take into account. At higher energies their contribution becomes larger and here we observe a clear justification of such a lack. It is also confirmed by the calculations in [2] where authors present predictions obtained with and without including relativistic effects and such a peak appears in the latter case.

Nevertheless my main goal is to describe deuteron photodisintegration at low energies and predictions seem to be well describing experimental data at $E_\gamma \lesssim 50$ MeV. The higher energies region is presented in order to investigate how far the predictions are from experimental results and what can be improved in the future (e.g. include relativistic part).

Maybe better reorganize figures, combine similar figures for different energies in one?

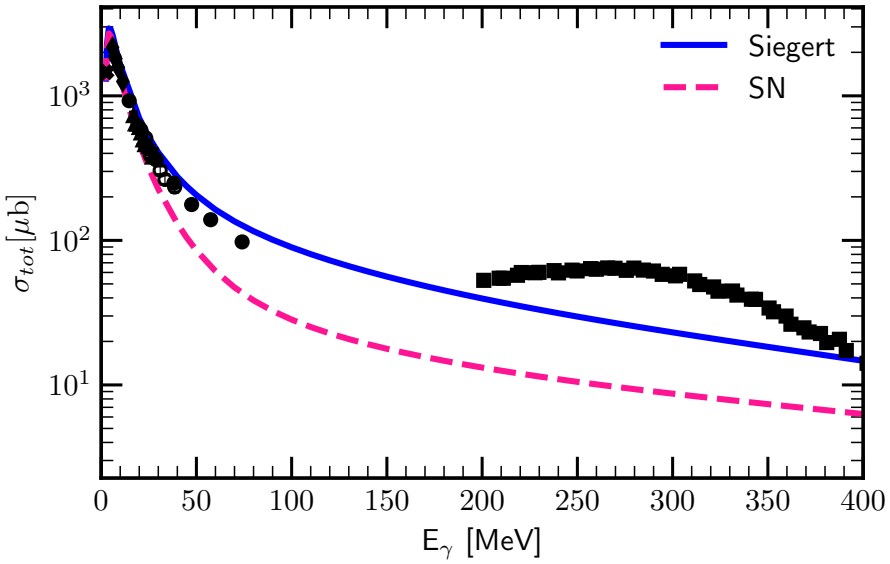

Figure 4.1: Total cross section as a function of the photon's energy E_γ. Solid blue line presents results obtained with SN+Siegert and dashed pink line - with only SN current. The experimental data are from [24] (black filled circles), [19] (empty circles), [20] (squares), [21] (triangles), [22] (cross "X") and [23] (dimonds).

Figures 4.3 - 4.5 show my predictions for the differential cross section $\frac{d\sigma}{d\Omega}$ at three values of the photon energy: 30, 100 and 140 MeV. They all are organized in a similar way: the left panel presents predictions obtained using SMS potential at different chiral orders (from LO to N^{4}LO+) with cut off parameter $L = 450$ MeV, the middle panel includes the truncation error's bands (described in Sec. 2.1) for each chiral order starting from NLO. And the right panel shows predictions obtained with different values of the cut off parameter at the chiral order N^{4}LO+.

Comparing the best predictions (N^{4}LO+, $\Lambda = 450$ MeV) for each of the Fig. 4.3 - 4.5 we can once more conclude that the higher photon's energy is, the larger is difference between the theoretical predictions and experimental measurements. At $E_\gamma = 30$ MeV (Fig. 4.3) my predictions almost perfectly match the data and the difference is almost always within the experimental uncertainties. Going to the energy 100 MeV (Fig. 4.4) the descriptions seems not to be such good: theoretical predictions match experimental data qualitatively, but the gap in the angles range ($60° < \theta_p < 130°$) is around 30% (check the value!). Looking at the Fig. 4.5 it is hard to say even about good qualitative description, the general trend of the angular dependance is presented, but still the predictions are far from experimental values. In addition, figures for each energy confirm the convergence of the predictions with respect to the chiral order. We see that the curves at LO are far from both experimental data and the best potential's predictions (N^{4}LO+) and the higher is photon's energy, the larger is this difference. With each subsequent chiral order, the curves are more closer to each other and the difference between N^{4}LO and N^{4}LO+ is hardly visible at current scale. So I can conclude that predictions are converged and further chiral orders would rather not bring large contribution to the cross section values. What may be helpful in a better data description is a 2N current and relativistic correction, mentioned earlier.

The middle pane of Fig. 4.3 - 4.5 presents theoretical (truncation) uncertainties and

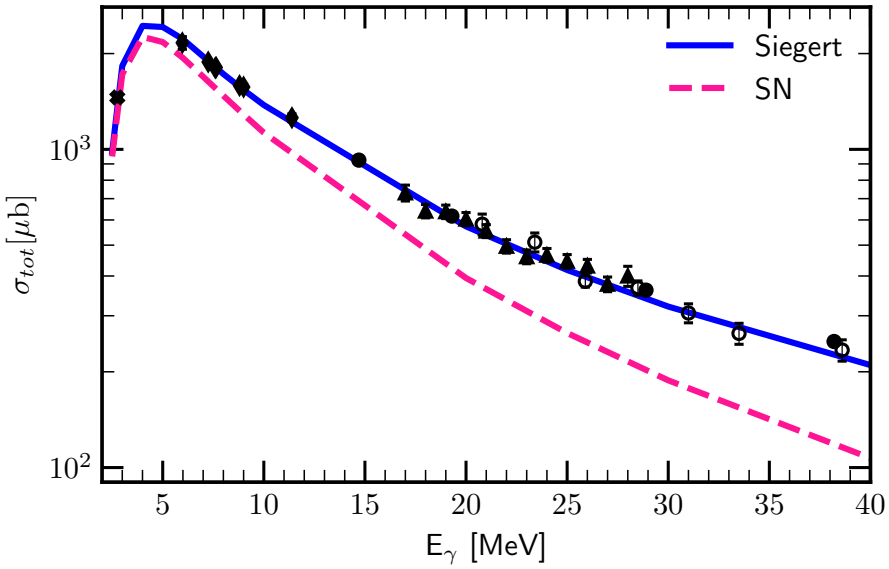

Figure 4.2: The same as on the Fig. 4.1 but for the energy range 2.5 - 40 MeV.

it once more confirm that for the regarded nuclear reaction chiral order N^{4}LO+ is able to produce converged predictions: the black band is hardly visible for the $E_\gamma = 30$ MeV and quit thin for larger energies. The difference with experimental data is rather systematic and is independent on the chiral order.

The right panes in discussed figures present a cut off dependency of my predictions. The ideal case is when the dependency is so weak that the choice of the parameter Λ would not make large changes. In practice the choice of this parameter can be important as it makes a noticeable difference in predictions.

On the Fig. 4.3 the cut off dependance is so weak, that, in fact, it all the lines (for different Λ values) overlap each other and we cannot see the difference with the naked eye. With increasing photon's energy to 100 and 140 MeV (Fig. 4.4 and Fig. 4.5) the spread becomes larger. Although the spread is visible, it is not so large and even for 140 MeV it is within 12%.

4.1.2 Tensor analyzing power

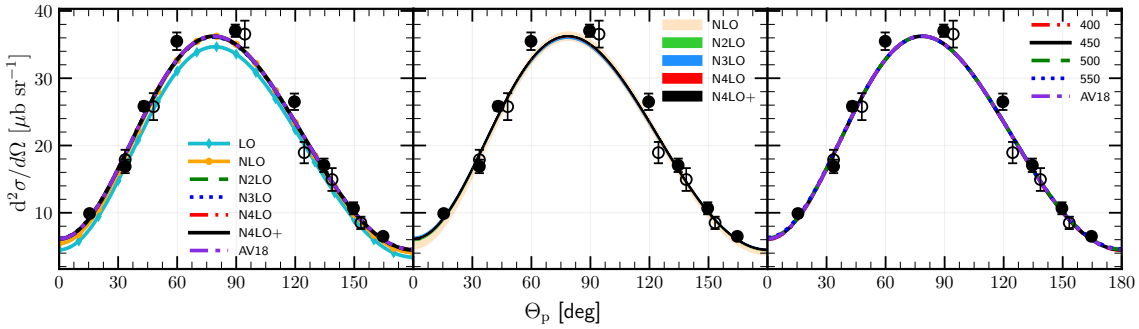

Figure 4.3: Differential cross section as a function of the outgoing proton angle in the center of mass frame for the photon's energy 30 MeV. Left figure presents results obtained using potential with different chiral orders (from LO to N^{4}LO+) with cutoff parameter Λ = 450 MeV whereas right figure presents a cutoff dependency and chiral potential N^{4}LO+ was used in all cases. For the sake of comparison, predictions obtained with AV18 potential are on both figures as well. Data points (filled and empty circles) are from [26].

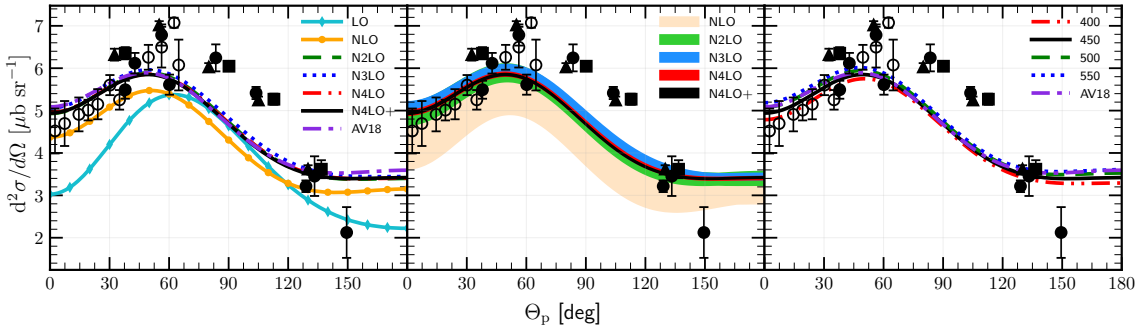

Figure 4.4: The same as on the Fig. 4.3 but for the photon's energy E$_\gamma$=100 MeV. All experimental data points (filled and empty circles, squares and triangles) are from [26].

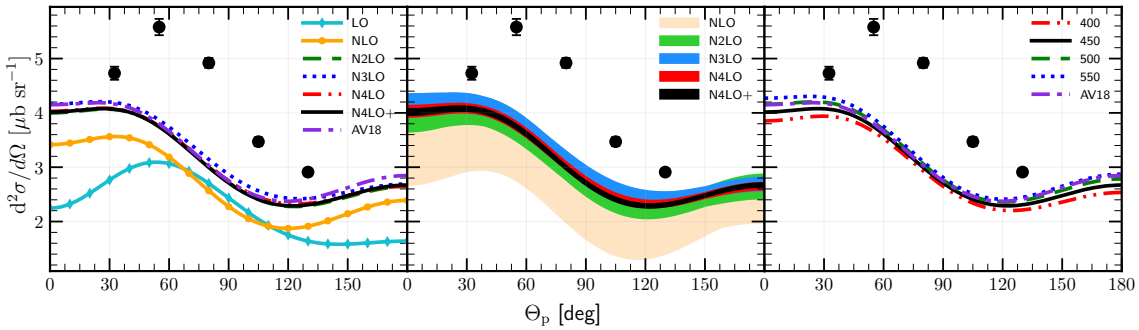

Figure 4.5: The same as on the Fig. 4.3 but for the photon's energy E$_\gamma$=140 MeV. The data are from [27].

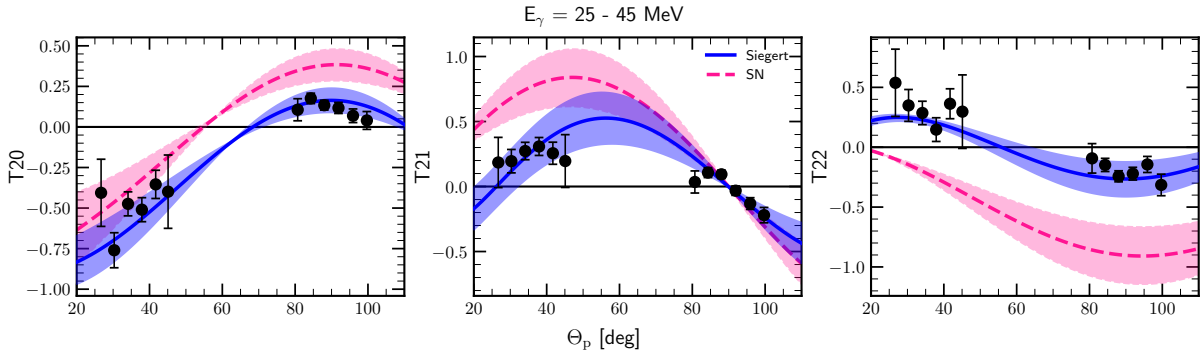

Figure 4.6: Tensor analyzing powers T_{20}, T_{21} and T_{22} as a functions of the outgoing proton angle θ_p (in the center of mass frame). Solid blue line is a mean value of my predictions obtained with a SMS potential at N^{4}LO+ chiral order and with $\Lambda = 450$ MeV at energy values from 25 to 45 MeV and where SN current was used together with Siegert approach. Pink dashed line is similar prediction but with SN only. The corresponding bands show the deviation of predictions in the regarded energy region. Filled circles are experimental data from [25] for the analogous energy span.

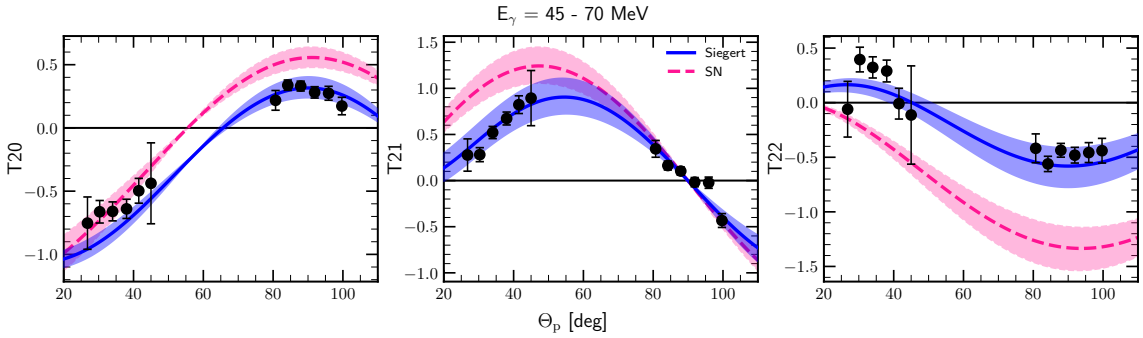

Figure 4.7: The same as on the Fig. 4.6 but for energy bin 45 - 70 MeV

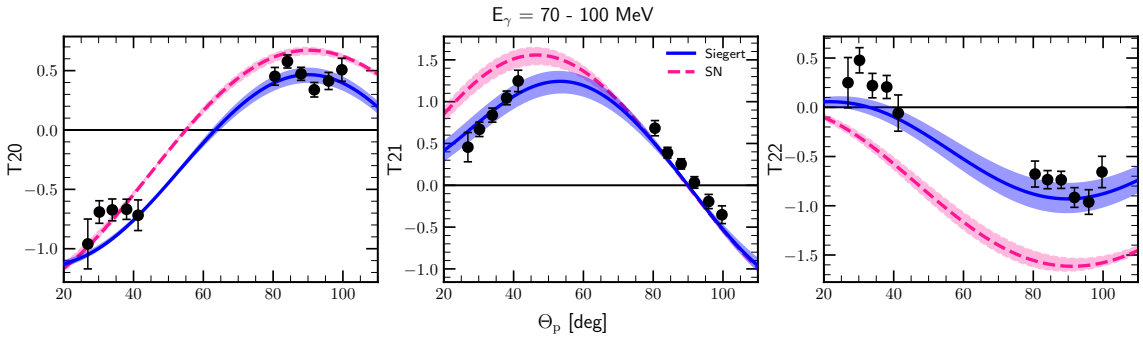

Figure 4.8: The same as on the Fig. 4.6 but for energy bin 70 - 100 MeV

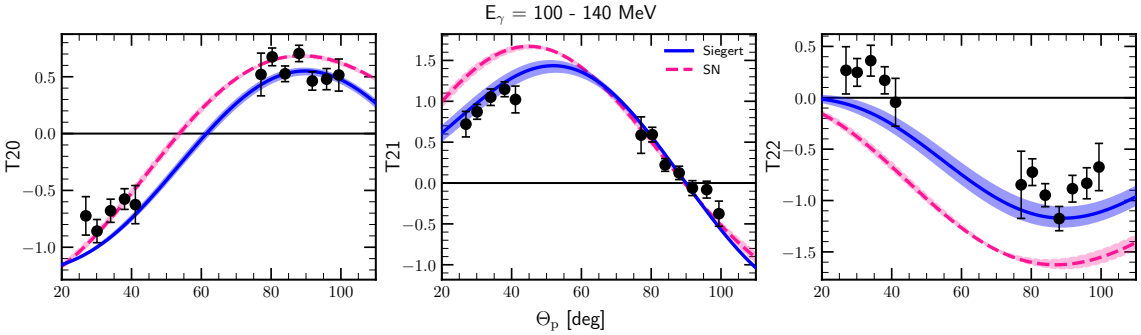

Figure 4.9: The same as on the Fig. 4.6 but for energy bin 100 - 140 MeV

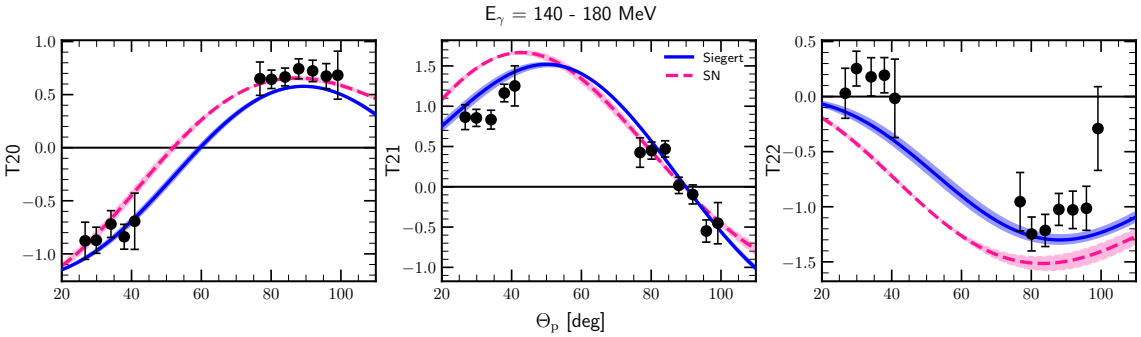

Figure 4.10: The same as on the Fig. 4.6 but for energy bin 140 - 180 MeV

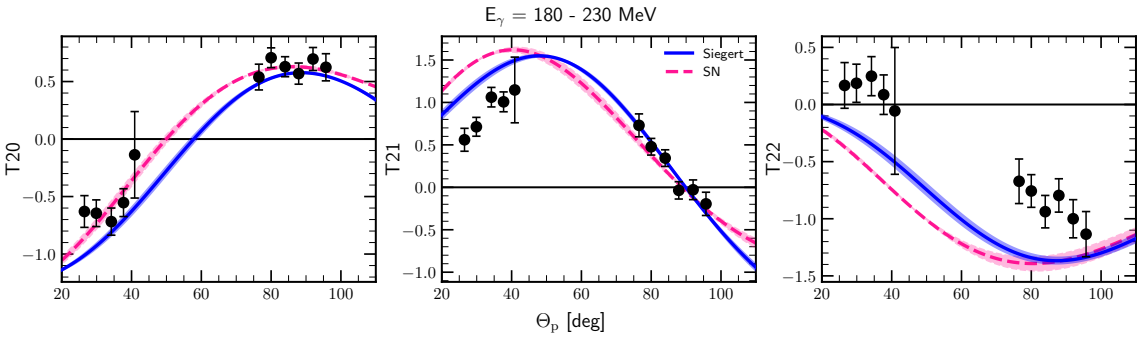

Figure 4.11: The same as on the Fig. 4.6 but for energy bin 180 - 230 MeV

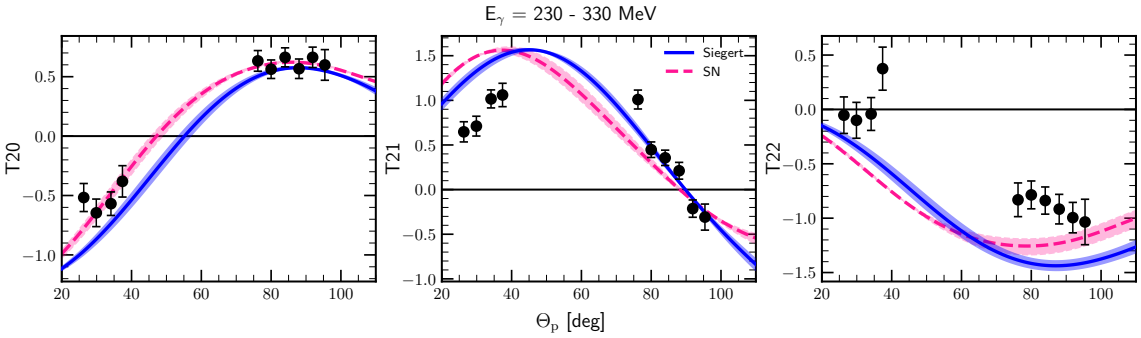

Figure 4.12: The same as on the Fig. 4.6 but for energy bin 230 - 330 MeV

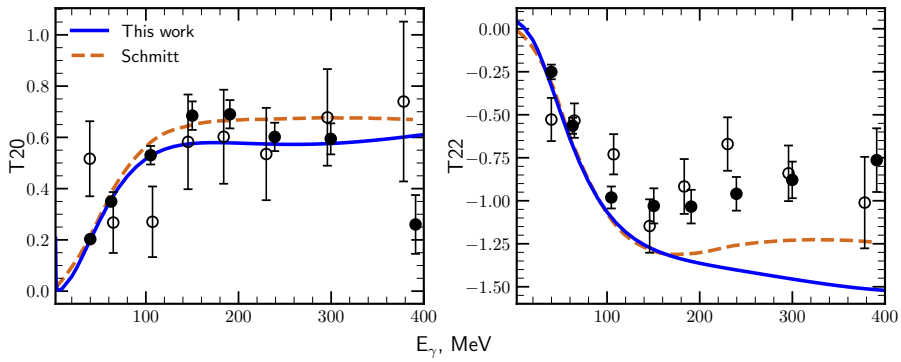

Figure 4.13: Tensor analyzing powers T_{20} and T_{22} as a functions of the photon energy E_γ with fixed outgoing proton angle $\theta_p = 88°$ (in the center of mass frame). My predictions (blue solid line) are obtained with SMS potential at chiral order N^{4}LO+ and with cutoff parameter $\Lambda = 450$ MeV. Dashed brown line presents calculations from [28]. Experimental data is taken from [25] (filled circles) and [29] (empty circles).

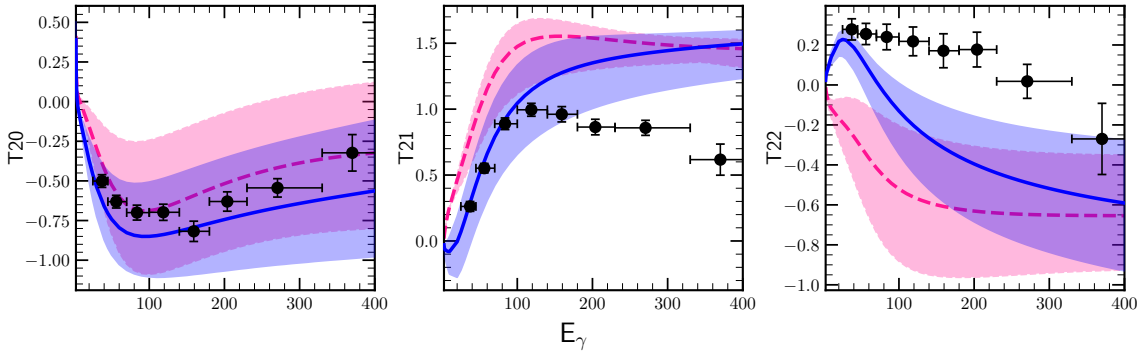

Figure 4.14: Tensor analyzing powers T_{20}, T_{21} and T_{22} as a functions of the photon's energy within the outgoing proton's angle range $24° - 48°$ (in the center of mass frame). Solid blue line is a mean value of my predictions obtained with SMS potential at N^{4}LO+ chiral order and with $\Lambda = 450$ MeV at energy values from 25 to 45 MeV within a given angles range and where SN current was used together with Siegert approach. Pink dashed line is similar prediction but with SN only. The corresponding bands show the deviation of predictions in the regarded energy region. Filled circles are experimental data from [25] for the analogous energy span.

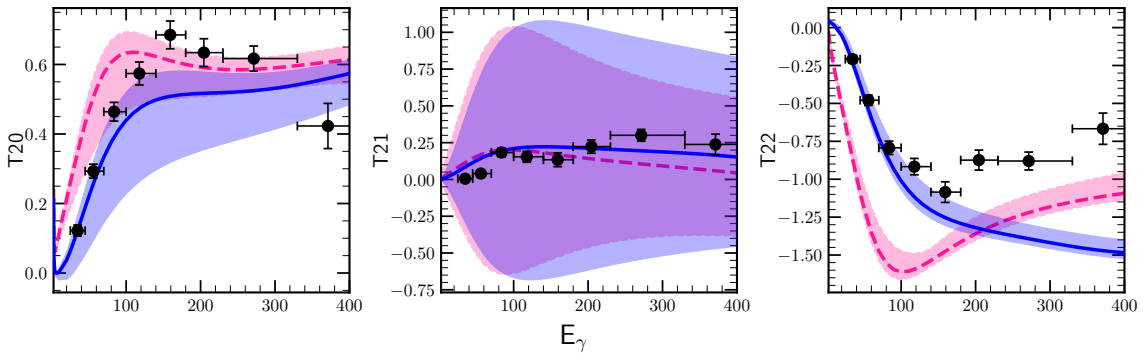

Figure 4.15: The same as on the Fig. 4.14 but for the angles' range $70° - 102°$.

BIBLIOGRAPHY

[1] B.L. Ioffe. Qcd (quantum chromodynamics) at low energies. *Progress in Particle and Nuclear Physics*, 56(1):232–277, 2006.

[2] H Arenhövel and M. Sanzone. Photodisintegration of the deuteron: A Review of theory and experiment. *Few Body Syst. Suppl.*, 3:1–183, 1991.

[3] W. Glöckle. Effects of the two-pion exchange three-nucleon force in the triton and 3he. *Nuclear Physics A*, 381(3):343–364, 1982.

[4] V. G. J. Stoks, R. A. M. Klomp, C. P. F. Terheggen, and J. J. de Swart. Construction of high-quality nn potential models. *Phys. Rev. C*, 49:2950–2962, Jun 1994.

[5] R. B. Wiringa, V. G. J. Stoks, and R. Schiavilla. Accurate nucleon-nucleon potential with charge-independence breaking. *Phys. Rev. C*, 51:38–51, Jan 1995.

[6] A. Nogga, H. Kamada, and W. Glöckle. Modern nuclear force predictions for the α particle. *Phys. Rev. Lett.*, 85:944–947, Jul 2000.

[7] Robert B. Wiringa, V. G. J. Stoks, and R. Schiavilla. An Accurate nucleon-nucleon potential with charge independence breaking. *Phys. Rev.*, C51:38–51, 1995.

[8] V. G. J. Stoks, R. A. M. Klomp, M. C. M. Rentmeester, and J. J. de Swart. Partial-wave analysis of all nucleon-nucleon scattering data below 350 mev. *Phys. Rev. C*, 48:792–815, Aug 1993.

[9] Steven Weinberg. Nuclear forces from chiral lagrangians. *Physics Letters B*, 251(2):288–292, 1990.

[10] Steven Weinberg. Effective chiral lagrangians for nucleon-pion interactions and nuclear forces. *Nuclear Physics B*, 363(1):3–18, 1991.

[11] R. Machleidt and D. R. Entem. Chiral effective field theory and nuclear forces. *Phys. Rept.*, 503:1–75, 2011.

[12] E. Epelbaum, H. Krebs, and U. G. Meißner. Precision nucleon-nucleon potential at fifth order in the chiral expansion. *Phys. Rev. Lett.*, 115(12):122301, 2015.

[13] P. Reinert, H. Krebs, and E. Epelbaum. Semilocal momentum-space regularized chiral two-nucleon potentials up to fifth order. *Eur. Phys. J.*, A54(5):86, 2018.

[14] Carl Gustav Jakob Jacobi. Ueber gauss neue methode, die werthe der integrale näherungsweise zu finden. 1826.

[15] Jun John Sakurai. *Modern quantum mechanics; rev. ed.* Addison-Wesley, Reading, MA, 1994.

[16] E Epelbaum, H Krebs, and U-G Meißner. Improved chiral nucleon-nucleon potential up to next-to-next-to-next-to-leading order. *Eur. Phys. J. A*, 51(5), May 2015.

[17] S. Binder et al. Few-nucleon systems with state-of-the-art chiral nucleon-nucleon forces. *Phys. Rev.*, C93(4):044002, 2016.

[18] Evgeny Epelbaum. High-precision nuclear forces : Where do we stand? *PoS*, CD2018:006, 2020.

[19] M. Bosman, A. Bol, J.F. Gilot, P. Leleux, P. Lipnik, and P. Macq. Measurement of the total cross section for the ^{1}H(n, γ) ^{2}H reaction between 37 and 72 mev. *Physics Letters B*, 82(2):212–215, 1979.

[20] J. Arends, H.J. Gassen, A. Hegerath, B. Mecking, G. Nöldeke, P. Prenzel, T. Reichelt, A. Voswinkel, and W.W. Sapp. Experimental investigation of deuteron photodisintegration in the δ-resonance region. *Nuclear Physics A*, 412(3):509–522, 1984.

[21] D. M. Skopik, Y. M. Shin, M. C. Phenneger, and J. J. Murphy. Photodisintegration of deuterium determined from the electrodisintegration process. *Phys. Rev. C*, 9:531–536, Feb 1974.

[22] R. Moreh, T. J. Kennett, and W. V. Prestwich. ^{2}H(γ,n) absolute cross section at 2754 kev. *Phys. Rev. C*, 39:1247–1250, Apr 1989.

[23] Y. Birenbaum, S. Kahane, and R. Moreh. Absolute cross section for the photodisintegration of deuterium. *Phys. Rev. C*, 32:1825–1829, Dec 1985.

[24] R. Bernabei, A. Incicchitti, M. Mattioli, P. Picozza, D. Prosperi, L. Casano, S. d'Angelo, M. P. De Pascale, C. Schaerf, G. Giordano, G. Matone, S. Frullani, and B. Girolami. Total cross section for deuteron photodisintegration between 15 and 75 mev. *Phys. Rev. Lett.*, 57:1542–1545, Sep 1986.

[25] I. A. Rachek, L. M. Barkov, S. L. Belostotsky, V. F. Dmitriev, M. V. Dyug, R. Gilman, R. J. Holt, B. A. Lazarenko, S. I. Mishnev, V. V. Nelyubin, D. M. Nikolenko, A. V. Osipov, D. H. Potterveld, R. Sh. Sadykov, Yu. V. Shestakov, V. N. Stibunov, D. K. Toporkov, H. de Vries, and S. A. Zevakov. Measurement of tensor analyzing powers in deuteron photodisintegration. *Phys. Rev. Lett.*, 98:182303, May 2007.

[26] S. Q. Ying, E. M. Henley, and G. A. Miller. DEUTERON PHOTODISINTEGRATION. *Phys. Rev.*, C38:1584–1600, 1988. including references.

[27] E. De Sanctis et al. Deuteron Photodisintegration Cross-section Between 100-MeV and 220-MeV. *Phys. Rev. Lett.*, 54:1639, 1985.

[28] K M Schmitt and H Arenhövel. Deuteron photodisintegration with the bonn OBE potentials. *Few-body syst.*, 7(3):95–117, 1989.

[29] S.I. Mishnev, D.M. Nikolenko, S.G. Popov, I.A. Rachek, A.B. Temnykh, D.K. Toporkov, E.P. Tsentalovich, B.B. Wojtsekhowski, S.L. Belostotsky, V.V. Nelyubin, V.V. Sulimov, and V.N. Stibunov. Measurement of the analyzing power components in photodisintegration of the polarized deuteron. *Physics Letters B*, 302(1):23–28, 1993.